Segregation of Mg, Cu and their effects on the strength of Al Σ5 (210)[001] symmetrical tilt grain boundary

Dongdong Zhao[a], Ole Martin Løvvik[b], Knut Marthinsen[a], and Yanjun Li[*,a]

[a]*Department of Materials Science and Engineering, Norwegian University of Science and Technology (NTNU), 7491 Trondheim, Norway*

[b]*SINTEF Materials and Chemistry, 0314 Oslo, Norway*

*Corresponding author.   E-mail: yanjun.li@ntnu.no   Tel.: +47 73551206

Abstract

Alien elemental segregation can pronouncedly change the grain boundary properties. Systematic first-principles calculations were performed to investigate the Mg and Cu segregation behavior at Σ5 (210)[001] symmetrical tilt grain boundary (STGB) in Al. The mechanical properties of Mg or Cu containing Σ5 (210)[001] STGBs were probed by combining a canonical Griffith fracture model with an *ab-initio* tensile test method. It is found that both Mg and Cu have a large driving force to segregate to Al grain boundaries, with Mg preferentially segregating at symmetric substitutional core sites and Cu at interstitial hollow sites at the grain boundary. Interestingly, Al Σ5 (210)[001] is shown to possess a stronger sink strength of Cu impurities than Mg. Both Mg and Cu segregation leads to a grain boundary expansion and a significant decrease of the grain boundary energy. Calculations show that Mg segregation leads to embrittlement of the STGB, contrary to the cohesion enhancing effect of Cu solutes on Al grain boundaries. The Mg induced embrittlement is due to a combination of "structural effect" – (grain boundary expansion) and "chemical effect" – (charge density depletion). The strengthening effect of Cu solutes lies in the creation of new Cu-Al bonds across the grain boundary, which is considered as a strong contribution to the grain boundary cohesion, thereby increasing its resistance against intergranular cleavage. This work demonstrates how a fundamental

theoretical understanding on the atomic and electronic level can rationalize mechanical properties of alloys at the macroscopic scale.

1. Introduction

Grain boundary segregation engineering (GBSE) has been considered as a promising routine for materials design [1-3]. Materials properties such as tensile strength, fracture toughness, conductivity, and corrosion resistance can be improved through manipulating GB properties in terms of structure, energy, mobility, and cohesion strength etc. via solute decoration. For instance, Li et al. [4], revealed that nanostructured steel fabricated by severe plastic deformation, has an extremely high tensile strength of 7 GPa, which was ascribed to the Gibbs segregation of carbon solutes to GBs. In aluminium alloys, Mg and Cu are two of the most important alloying elements, having strong solute strengthening effects. Accordingly, Cu-rich 2xxx and Mg-rich 5xxx Al alloys are widely used in structural applications in aerospace and automotive fields as high strength and lightweight materials. Numerous experimental works have shown that Mg and Cu solutes have strong tendency to segregate towards Al GBs [5-12]. As an example, Sha et al. [12] showed that a strong segregation of Mg and Cu towards GBs in an ultrafine grained (UFG) Al–Zn–Mg–Cu alloy can stabilize the grain size. A number of theoretical studies have investigated the effect of Mg segregation on the cohesion of Al GBs [13-18]. Still, it remains a controversy whether Mg solutes would weaken or strengthen Al GBs. For instance, both Zhang et al. [17] and Razumovskiy et al. [18] predicted a modest cohesion enhancing effect for Mg upon Σ5 (210) STGB, contrary to the results by Song et al. [13] and Liu et al. [14], in which Mg was demonstrated to decrease the cohesion strength of Al GBs. In addition to solute strengthening, Cu is known to strengthen Al alloys by forming coherent precipitates. However, the effect of Cu solute on the cohesion strength of Al GBs is largely unclear. No comprehensive work has been reported on the effect of Cu segregation on Al GBs cohesion. A systematic investigation is thus needed to clarify the effect of Mg and Cu doping on the strength of Al GBs.

Generally, a segregated impurity element may act to enhance cohesion or increase embrittlement of GBs in alloys [19-23]. For instance, Bi (bismuth) segregation to Cu GBs has been demonstrated to promote GB embrittlement [24, 25]. In contrast, B (boron) is known, both experimentally and theoretically, to be a universal cohesion enhancer for GBs in many metals, e.g. Fe [26], Ni [27], and Al [28]. Two thermodynamic approaches are widely adopted to evaluate the

embrittlement or strengthening potency of impurities on GBs: the canonical Griffith model [29] and the grand-canonical Rice-Wang model [30]. Both methodologies describe the effect of impurities on GB cohesion from an energetic perspective. Generally, if the segregation of an impurity energetically favors the GB over free surface, the resistance of GB against brittle intergranular fracture will be improved; on the contrary, an impurity element which energetically favors free surface more than GB would increase the susceptibility of GB towards brittle intergranular fracture. Although these two models are successful in predicting cohesion strength of various GBs, they are, however, different in the way of treating segregated impurities. Recently, Bauer et al. [31] adopted both models to address the Zn induced embrittlement on Fe GBs and found that Zn-induced GB weakening potency was dependent upon the choice of models. One other prevalent approach to evaluate the impurity segregation effect on GB strength is the *ab initio* tensile test, which depicts the response of GB against uniaxial tensile strain on the atomic level. Under applied stresses, valuable insights into the mechanism and behavior of impurity and host atoms can be obtained in terms of relaxed atomic and electronic structures, bonding characteristics, etc. Detailed analysis of the calculated binding energy-displacement data can provide important information, i.e. fracture energy, theoretical tensile strength etc. of the GBs. A variety of works [32-35] have demonstrated the efficiency of this methodology.

In the present work, a systematic research is undertaken to probe the segregation behavior of Mg and Cu solutes and their doping effect upon the GB strength of Al, within the framework of canonical Griffith fracture model aided with *ab-initio* tensile test calculations. A relatively simple $\Sigma5$ (210)[001] symmetrical tilt grain boundary ($\Sigma5$ (210) STGB) is used as an example. We firstly revisited the structural and energetic properties of Al $\Sigma5$ (210) STGB. Then, the energetically favorable segregation sites for Mg and Cu atoms in the GB were determined and the corresponding segregation energy was calculated. Hereafter, the Griffith fracture model was adopted to calculate the fracture energy of Al $\Sigma5$ (210) STGBs segregated with Mg and Cu. Following that, *ab-initio* tensile test calculations were performed to gain insight into the fracture behavior of Mg and Cu segregated Al $\Sigma5$ (210) STGBs. In a last part of the work, the relaxed atomic and electronic structures, as well as

4

tensile test data were utilized to determine the underlying role that Mg and Cu solutes played in the embrittling and strengthening effect upon Al GBs.

2. Models and methods

2.1 First-principles calculations

The first-principles calculations in the present work were carried out using Vienna ab initio simulation package [36, 37]. A projector augmented wave method was employed to describe the electron-ion interactions [38, 39]. The exchange correlation potential was treated using the generalized gradient approximation (GGA) in the Perdew–Burke–Ernzerhof form [40]. We used a cutoff of 350 eV for all the calculations to insure that the total energy differences were less than 1 meV/atom. A k-points sampling of $6 \times 6 \times 3$ within the Monkhorst-Pack scheme [41] in combination with the linear tetrahedron method including Blöchl corrections [42] was used for the reciprocal-space energy integration in the Brillouin zone (BZ). The convergence criteria for total energy and forces were chosen as 10^{-6} eV and 10^{-2} eV/Å, respectively, in the relaxation process.

2.2 Grain boundary models

In the present work the representative Al $\Sigma 5$ (210) STGB was selected and constructed based on the coincidence site lattice (CSL) approach. Herein, (210) and [001] denote the habit plane and crystal Miller indices of the tilt axis for the GB model. Figure 1 represents the atomic crystal structures of the pristine $\Sigma 5$ (210) STGB without segregation and with one monolayer Mg (GB/1ML-Mg) or Cu (GB/1ML-Cu) segregation (four impurity atoms segregated at the GB forms one mono-layer). Each supercell contains 20 layers of (210) planes stacking in the direction perpendicular to the GB plane, two GBs due to the periodicity, as well as two micro grains, as sketched in Fig. 1. The stacking grains are periodic along the c directions, tilted with respect to the [001] direction. This stacking sequence is reversed after a half period along the c direction, forming the mirror symmetry in the CSL GB model. The misorientation (tilt) angle between the micro grains in the $\Sigma 5$ STGB structure is 36.9°, which is in the category of High Angle Grain Boundary (HAGB) misorientation. The initial

GB configuration before atomic relaxations has cell length of $(2, \sqrt{5}, 2\sqrt{5})a_0$, with a_0 being the lattice constant of Al. Note that the energy profile as a function of the rigid shift of micro grains parallel to the GB plane has been determined to make sure that the Σ5 (210) STGB structure is actually the stable GB configuration.

The most energetically favorable adsorption site of Mg or Cu atom along the GB was firstly determined. Interestingly, we found that substitutional segregation is more favorable over interstitial segregation for Mg solutes (cf. Fig. 1(a)), given its congenial atomic size to Al. However, Cu is prone to occupy the interstitial hollow site at the GB (cf. Fig. 1(a)), similar to the segregation behavior of C atoms to Mo and Fe Σ5 STGBs [43], as well as B solutes to Al Σ5 STGBs [28]. Calculations show that the Al Σ5 (210) STGB stays symmetric with the segregation of Mg and Cu atoms.

2.3 Tensile test calculations

Ab initio tensile test calculations for the Al Σ5 (210) STGBs were carried out in the framework of rigid-grain-shift (RGS) methodology and RGS + relaxations [44, 45]. First, the equilibrium GB supercell was elongated with small displacement increment in the direction perpendicular to the GB plane (along [210] direction in Fig. 1(a)). At each displacement distance, GB separation was manually inserted between Grain1 and GB1, Grain2 and GB2 (cf. Fig. 1(a)) to accommodate the cell length change (note that the separations should be equal). For each displacement distance, two kinds of calculations were performed, i.e. (1) RGS, without subsequent atomic relaxations; (2) RGS + atomic relaxations, which were implemented with the cell length fixed. As a consequence, two kinds of binding energy-displacement data can be obtained. More details about the calculation methodology can be found in Ref. [43, 46].

3. Results

3.1 Energetic properties of Al Σ5 (210) STGB

The GB energy γ_{GB} of a pristine Σ5 (210) STGB is calculated as

$$\gamma_{GB} = \left(E_{AlGB}^{tot} - N_{Al}\mu_{Al} \right) / 2A \tag{1}$$

Here, E_{AlGB}^{tot} is the total energy of the GB simulation supercell as illustrated in Fig. 1(a) and N_{Al} the same number of Al atoms. μ_{Al} is the chemical potential per Al atom, which is taken from *fcc* Al. A is the area of GB in the supercell. The scaling factor ½ in Eq. (1) is due to the presence of two GBs in the supercell. The presently determined γ_{GB} of Σ5 (210) STGB is 0.518 J/m^2 at 0 K. Table 1 collects the previously theoretical and experimental values for γ_{GB}. It is evident that the present γ_{GB} agrees well with the previous theoretical results, ranging from 0.411 to 0.502 J/m^2 [18, 47-49] and is also consistent with the experimental measurements of 0.600 J/m^2 [50], 0.380 J/m^2 [51].

When fracture occurs to the Σ5 (210) STGB, two free (210) surfaces would be created. The surface energy γ_{surf} is actually the energetic penalty that is needed to produce free surfaces from breaking a single crystal or equivalently a GB, which is evaluated through Eq. (2) [31] in the present work.

$$\gamma_{surf} = \left(2E_{AlFS}^{tot} - N_{Al}\mu_{Al} \right) / 4A \tag{2}$$

Herein, E_{AlFS}^{tot} is the total energy of the fractured GB simulation supercell, the scaling factor ¼ accounts for the four free (210) surfaces formed after the fracture of two GBs in the supercell. Our calculated γ_{surf} yields a value of 1.041 J/m^2, being in good agreement with the experimental results of 0.980 J/m^2 at 723 K [51] and 1.150 J/m^2 at 298 K [51], as well as the theoretical predictions of 1.016 J/m^2 [49] and 0.96 J/m^2 [18] (See Table 1).

The fracture energy Δγ of a GB, also interpreted as the work of separation (WoS), is defined as the energy penalty needed for the intergranular fracture of a GB into two free surfaces and can be calculated via the following

$$\Delta\gamma = 2\gamma_{surf} - \gamma_{GB} \tag{3}$$

The factor 2 indicates the two free surfaces after the fracture of a GB. The presently calculated fracture energy $\Delta\gamma$ of $\Sigma 5$ (210) STGB is 1.568 J/m^2, being consistent with the theoretical evaluations of 1.531 J/m^2 [49], 1.44 J/m^2 [18], and also agrees with the experimental value of 1.92 J/m^2 [51].

A first-principles uniaxial tensile test of pristine $\Sigma 5$ (210) STGB was performed with an aim to get insight into its mechanical behavior. Initially, to model the ideal brittle cleavage, the micro grains were treated with RGS methodology [44, 45]. The implementation of RGS approach to the pristine $\Sigma 5$ (210) STGB can provide us a set of energy-displacement data, which can be fitted using the universal binding energy relationship (UBER) [44, 45], originally postulated by Rose et al. [52] and terming by

$$E_b(\delta) = g(a) \cdot \left| E_b^e \right| \tag{4}$$

$$g(a) = -(1+a) \cdot e^{-a} \tag{5}$$

Wherein $g(a)$ is the universal function, E_b^e is the binding energy at the equilibrium displacement, a is the rescaled displacement, defined with the characteristic length scale l

$$a = \frac{\delta}{l} \tag{6}$$

$$l = \sqrt{\frac{\left| E_b^e \right|}{E_b^{"}(\delta_0)}} \tag{7}$$

Via differentiating the fitted energy-displacement data, the theoretical tensile strength of the pristine $\Sigma 5$ (210) STGB can be evaluated [44, 45],

$$\sigma_{th} = \frac{dE}{d\delta} \tag{8}$$

Herein, δ corresponds to the displacement and the maximum tensile strength can be calculated at the inflection point. In contrast to the RGS methodology, the relaxed cleavage approach i.e. RGS +

subsequent relaxations [45] was also employed to study the mechanical response of Σ5 (210) STGB. This approach allows us to release the elastic energy during the atomic relaxations.

Figure 2 shows the binding energy versus displacement curves of pristine Σ5 (210) STGB, evaluated by the RGS and RGS + relaxation methodology. One can see that the RGS methodology produces a continuous binding energy versus displacement curve, with the minimum of which giving us the equilibrium binding energy E_b^e [43]. During tensile deformation, the absolute value of binding energy firstly decreases sharply with increasing displacement, then this decrease slows down until it saturates to the energies of fractured free surfaces at larger displacement distances (i.e. > ~ 4 Å). Moreover, it is found that the UBER fits the RGS results well; consequently, the fracture energy and theoretical strength of Al Σ5 STGB can be predicted using the regressed UBER curve.

From Fig. 2, one can also find that the relaxed binding energy versus displacement curves of pristine Al Σ5 (210) GB does not abide by the UBER uniformly all through the displacement. Apparently, there are three distinct regions in the relaxed binding energy curves (see Fig. 2): (i) for small displacements $\delta < l_h$, the precrack introduced in the atomic structure will be healed up and the prefractured surfaces will be reconnected as a result of elastic relaxations during the calculations. The binding energy curve for $\delta < l_h$ is always continuous and has parabolic feature; (ii) crack openings between l_h and l_f ($l_h < \delta < l_f$), represent the instability region, in which the precrack initially introduced in the atomic structures can no longer be healed up. This abrupt breakup of the atomic bonds between the fractured surfaces results in the discontinuity of the curve and it is in such a region that the accurate binding energy can't be calculated; (iii) at larger displacements ($\delta > l_f$), the prefractured surfaces are stable and attracted to their corresponding micro grains, forming the cracks and a repeated slab configuration. In this region, the binding energy curve is again continuous, and the energy decreases slowly with the displacement until it reaches the energies of fractured free surfaces of Σ5 (210) STGB at sufficiently large separation distance. A well UBER fitting of continuous curves (for $\delta < l_h$ and $\delta > l_f$) was conducted for the sake of finding the equilibrium binding energy E_b^e,

theoretical strength etc. Through a comparison between the RGS and RGS + relaxation binding

energy curves, we found that atomic relaxations would reduce E_b^e of Σ5 (210) STGB by 0.196 J/m^2,

which is in nice agreement with the theoretical value of 0.2 J/m^2 by Ref. [49]. It is proposed that this

decrease is attributed to the internal stress released via relaxations of the GB structure.

3.2 Mg and Cu segregation to Al Σ5 (210) STGB

A: Grain boundary energy, segregation energy of Mg and Cu in Al Σ5 (210) STGB

The γ$_{GB}$ of the Mg or Cu containing Al Σ5 (210) STGBs is calculated with following equation,

$$\gamma_{GB} = \left(E_{f@AlGB}^{tot} - N_{Al}\mu_{Al} - N_f\mu_f \right)/2A, \quad f = Mg, Cu \qquad (9)$$

Where $E_{f@AlGB}^{tot}$ is the total energy of GB in the simulation supercell containing N_f Mg or Cu atoms

with chemical potential μ_f at the interface. μ_f is taken as the values from the respective bulk

calculations of Mg and Cu. Here, scaling factor ½ in Eq. (9) again indicates the presence of two GBs

in the simulation supercell.

Using Eq. (9), we calculated the γ$_{GB}$ of Σ5 (210) STGBs as a function of coverage (x ML, 0<x

≤ 1) of Mg or Cu atoms segregated at the interface. One can find in Fig. 3(a) that Mg or Cu can both

decrease the γ$_{GB}$ of Σ5 (210) STGB. A higher coverage of Mg or Cu atoms segregated at the GB

would result in a lower γ$_{GB}$ (see Table 2). 1ML Mg residing at the GB can induce a 40% reduction of

γ$_{GB}$. Furthermore, Cu has a more significant reducing effect upon γ$_{GB}$ than Mg. It is interesting to see

in Fig. 3(a) that 1ML coverage of Cu atoms at the GB would decrease γ$_{GB}$ down to a negative value.

In fact, the 1ML Cu atoms at Σ5 (210) STGB in the supercell corresponds to an average Cu

concentration of 10%, which is far beyond the maximum solubility limit of Cu in Al matrix, which

means a rather high chemical potential of Cu atoms in Al bulk in Eq. (9) and therefore a low γ$_{GB}$. Note

that the negative γ$_{GB}$ has been discussed by Kirchheim [53, 54] and Millett et al. [55, 56] as being a

metastable equilibrium state, which might be achieved in nano-crystalline materials with certain

amount of solute. There is also another possibility that under such a high local concentration of Cu, AlCu intermetallic particles, for instance, θ–Al₂Cu, may precipitate in the GB. Still, further definitive study is needed to clearly address this problem. The substantial reduction of γ_{GB} induced by the segregation of Mg or Cu does not necessarily represent the increase of GB cohesion strength since the segregated Mg or Cu solutes also affect γ_{surf}, which is to be discussed in a latter part.

To gain insight into the segregation tendency of Mg or Cu atoms towards Al Σ5 (210) STGB, a segregation energy γ_{seg} can be evaluated with Eq. (10) in terms of the following

$$\gamma_{seg} = E^{GB} - E^{Bulk} \tag{10}$$

E^{GB} is the impurity energy of Mg or Cu at GB, and E^{Bulk} correspondingly in bulk, both of which can be calculated as

$$E^{GB} = E_{GB/f_x} - E_{GB} - x \cdot \mu_f \,, \ f = Mg, Cu \tag{11}$$

$$E^{Bulk} = E_{Bulk/f_x} - E_{Bulk} - x \cdot \mu_f \,, \ f = Mg, Cu \tag{12}$$

E_{GB/f_x}, E_{Bulk/f_x} are the total energy of GB simulation supercell or bulk with x Mg or Cu impurity atoms, E_{GB} and E_{Bulk} stand for the total energy of pristine GB and pure Al bulk without impurities, respectively. A negative value of γ_{seg} would indicate that impurity atoms prefer to segregate towards GB from the bulk environment. Figure 3(b) displays the variation of γ_{seg} for Mg and Cu versus the impurity content. As can be seen that γ_{seg} remains negative throughout the impurity coverage range, for both Mg and Cu. Furthermore, Cu bears a more negative γ_{seg} than Mg (cf. Table 2 and Fig. 3(b)), which is a sign of Σ5 (210) STGB possessing higher sink strength of Cu impurities than Mg.

B: Fracture energy of Σ5 (210) STGBs with Mg, Cu segregations

In the present work, the canonical Griffith model is implemented to capture more insight into the variation of the fracture energy Δγ of Σ5 (210) STGB originated from Mg or Cu segregation.

Within this model, the impurity atoms present along the GB is distributed at the fractured surfaces following the cracking process and the total amount of impurity atoms is kept conserved.

The evolution of (210) Al free surface energy as a function of the segregation of Mg or Cu atoms can be evaluated by

$$2\gamma_{surf} = \left(2E^{tot}_{f@AlFS} - N_{Al}\mu_{Al} - N_f\mu_f \right)/2A, \ f = Mg, Cu \qquad (13)$$

with $E^{tot}_{f@AlFS}$ representing the total energy of (210) Al surface with Mg or Cu segregation. Prior to the *ab initio* tensile test calculations of GB supercell, one has to determine the most energetically favorable distribution of foreign solutes at the two fractured surfaces after GB cleavage. It is interesting to find that substitutional Mg solutes energetically favor an even split-up following the fracture of GB and resides symmetrically at the two newly-formed surfaces. However, it is a different case for the interstitially segregated Cu atoms, which always prefer to attach to one of the newly-generated surfaces. As displayed in Fig. 4(a), γ_{surf} decreases substantially along with the increase of Mg and Cu coverage, both in RGS and RGS + relaxation methodology. This reduction can be ascribed to the binding energy between Mg or Cu solutes and surfaces [31]. By comparing with RGS, we also find that RGS + subsequent relaxation methodology produces a lower surface energy throughout the coverage range (cf. Fig. 4(a) and Table 2).

Based on the calculated γ_{GB} and the corresponding γ_{surf} as collected in Table 2, the fracture energy $\Delta\gamma$ of Mg or Cu containing $\Sigma5$ (210) STGBs, are predicted using Eq. (3) and displayed in Fig. 4(b), as a function of Mg or Cu coverage. As indicated in Fig. 4(b), RGS approach always predicts a larger fracture energy $\Delta\gamma$ relative to RGS + relaxation methodology. Focusing on the alloying effects, one can find that the presence of Mg at GB does not alter $\Delta\gamma$ much, i.e. slightly cuts down $\Delta\gamma$ in RGS case with increase of Mg content and keeps $\Delta\gamma$ as more or less constant throughout the Mg coverage within RGS + relaxation methodology (cf. Fig. 4(b) and Table 2). This however, does not necessarily mean that foreign Mg solutes will impose negligible effect upon the cohesion strength of $\Sigma5$ (210) STGB since in this case $\Delta\gamma$ alone is not sufficient to depict the fracture behavior of GBs [43]. A

significant increase of Δγ with increasing interstitial Cu segregation at the GB is observed, both in RGS and RGS + relaxation cases (cf. Fig. 4(b)). Compared with pure Σ5 (210) STGB, 1 ML Cu coverage can produce a 30% increase in Δγ (RGS + relaxation, cf. Table 2), suggesting Cu segregation would efficiently enhance the resistance of Al GB towards intergranular fracture.

C: Scaling of energy-displacement curves

Rose et al. [52] has proposed that cohesion or binding energy E_b of metals has a universal form terming by Eq. (4). Figure 5(a) and (b) display the rescaled binding energy displacement curves based on Eq. (4) of Mg (a) and Cu (b) segregated Σ5 (210) STGBs, which are evaluated via RGS methodology. One can find that the rescaled data of Cu segregated GB fits perfectly onto one UBER curve, bearing fine universality (see Fig. 5(b)). It is, however, not the case for GBs segregated with Mg solutes, where an evident data scattering in the displacement range of 1 to 4 Å (cf. Fig. 5(a)) makes it difficult to fit all data points uniformly with Eq. (4). It is supposed that the interactions between impurity solutes on opposite sides of the fractured surfaces induced by a symmetric distribution of substitutional Mg solutes during the onset of intergranular fracture have led to the non-universality of binding energy-displacement data. In contrast, such interactions do not exist for the one-side preferentially Cu-segregated surfaces, producing the finely shared universality of the binding energy-displacement curves for Σ5 (210) STGBs with Cu segregations.

D: Theoretical tensile strength

Fig. 6(a) and (b) present the theoretical strength of Σ5 (210) STGBs with Mg and Cu segregation, as well as the (210) planes in bulk Al as a function of displacement, obtained by the RGS methodology. Each tensile strength curve has a peak value corresponding to σ_{max}, the maximum tensile strength, which are collected in Table 3. Regarding Fig. 6(a), one can find that the pure Al (210) planes exhibit the highest σ_{max}, i.e. 11.96 GPa, higher than the strength of the pristine Al Σ5 (210) STGB (10.86 GPa). This feature is consistent with the result by Janisch et al. [45] that the strength of GB is generally lower than that of bulk planes in the corresponding orientation. It is worth noting that the presently determined strength of both Al bulk (210) planes and pristine Σ5 (210)

STGB is in good coincidence with the results by Zhang et al. [49] (cf. Table 3). Furthermore, Fig. 6(a) sheds lights upon the weakening potency of Mg towards Σ5 (210) STGB. As indicated in Fig. 6(a) and Table 3, the theoretical strength of Mg segregated GBs monotonically decreases with increase of Mg content residing at the GB interface, i.e. from 10.33 to 8.88 GPa (cf. Table 3). As discussed in Section B, Mg solutes exert negligible effect on Δγ of Σ5 (210) STGB, while the Mg-induced reduction in theoretical strength of Σ5 (210) STGB may lead to the conclusion that fracture energy alone is not adequate to depict the intergranular fracture behavior of GBs. In addition, energy-based theoretical models used for describing the intergranular fracture, e.g. Griffith model, Rice-Wang model etc., may have controversies between each other even they're utilized to depict the same system [31]. Hence, a complex approach combining fracture energy calculation and theoretical strength analysis, which is also recommended by Tahir et al. [43], would be necessary for the description of intergranular fracture behaviors of GBs.

Figure 6(b) presents the theoretical strength-displacement curves of Σ5 (210) STGBs with Cu segregation. As indicated, the slopes of the strength-displacement curves slightly increase with the increased coverage of Cu solutes at GB. Besides, one can furthermore find that with accumulating Cu content, the maximum tensile strength σ_{max} continuously increases, i.e. from 11.37 (0.25 ML) to 13.29 GPa (1 ML) (cf. Table 2), revealing that Cu has a strengthening effect upon Σ5 (210) STGB. Note that this GB strengthening originated from Cu segregation is not surprising given the fact that Cu solutes can significantly increase the fracture energy Δγ of Σ5 (210) STGB, as discussed in the former part. Therefore, alien Cu solutes appear to be an attractive cohesion enhancer for Al GBs.

A traction separation analysis based on the cohesive zone model can be carried out upon the strength-displacement curves, where we can determine the critical separation δ_c at the maximum tensile strength point. The final separation δ_f, which represents the absolute splitting of the fractured surfaces, can also be evaluated via the following equation [43, 57]

$$\delta_f = \frac{2\Delta\gamma}{\sigma_{max}} \tag{14}$$

The calculated δ_c and δ_f of the GBs with different Mg or Cu coverage are as collected in Table 3. An increased δ_c and δ_f along with the increment of Mg coverage at the GB would suggest that Mg segregation would decrease the rigidness and stiffness of $\Sigma 5$ (210) STGB (cf. Fig. 7). The authors believe that this decreased stiffness is ascribed to the change in bonding nature induced by Mg segregation. However, such evident trend of δ_c and δ_f is not observed for GBs with Cu segregation.

Since RGS + relaxation methodology provides us with a distinguished binding energy-displacement curve, a distinct theoretical strength-displacement correlation can be obtained. Figure 8 displays the relaxed theoretical strength of Al bulk (210) planes, pristine $\Sigma 5$ (210) STGB, GB/1ML-Mg and GB/1ML-Cu, with σ_{max} of these curves as collected in Table 3. Each curve starts with elastic regime in which the strength versus displacement follows Hook's law. At certain critical displacements between 2 to 3 Å, sharp drops corresponding to the abrupt breakup of GBs occur in these strength curves. Focusing on σ_{max}, one can find that elastic relaxations have the influence of lowering down the theoretical tensile strength, compared with RGS method, in which the strain determining the strength is localized between the defined fracture planes at the GB. Upon relaxation, the localized elastic energy would be released and the theoretical strength would saturate and decrease as a result of the rearrangement of atoms, thereby the determined theoretical strength by the RGS + relaxation approach is an overall strength of the simulation supercell. Still, elastic relaxations do not change the relative magnitude of tensile strength, GB/1ML-Cu was predicted to possess the highest σ_{max}, i.e. 10.37 GPa, larger than that of Al bulk (210) planes (9.39 GPa, cf. Table 3), verifying the Cu strengthening effect upon the GB. The weakening potency of Mg towards $\Sigma 5$ (210) STGB was reproduced with GB/1ML-Mg, exhibiting the lowest calculated σ_{max}, i.e. 7.79 GPa, smaller than that of pristine $\Sigma 5$ (210) STGB (8.93 GPa). It is worth noting that M. Černý et al. [58] have made an attempt to incorporate the Poisson's contraction in the *ab initio* tensile test, which shows that inclusion of Poisson's effect in uniaxial tensile loading produces much lower theoretical strength compared with the RGS methodology. However, due to the limited number of atoms in the supercell (a semi-infinite system) used in the calculations, the Poisson's contraction has not been considered in the present *ab initio* tensile test.

E: Charge density

Charge accumulation and depletion would result in strengthening and weakening of interatomic bonds, respectively. Herein to get a better understanding of the strength change of Σ5 (210) STGBs due to the segregation of Mg or Cu solutes, we investigated the charge density evolution of different GBs during the onset of uniaxial tensile test. Figures 9-11 present the contour plots for the charge densities in the [001] projection of pristine Σ5 (210) STGB, GB/1ML-Mg and GB/1ML-Cu respectively during straining at different displacements. As shown in Fig. 9, strong bonding forms between atoms Al(2) and Al(-2) after atomic relaxation, which contributes primarily to the bonding strength of GB. With increased straining before fracture along the [210] direction, interlayer bonding weakens fast along the [110] direction. The bonds linking the GB are still connecting until the separation displacement of 2 Å, sharing a nice agreement with the result by Zhang et al. [49], which is 3.7 a.u. (1.96 Å). It is speculated that the instant break of interatomic bonds Al(2)-Al(-2), Al(1)-Al(2) and Al(1)-Al(4) happens between displacement 2 and 2.1 Å. At displacement 2.1 Å, the GB is already fractured. The interlayer bonding along the [111] direction recovers by relaxation after the fracture of GB. At displacement above 2.1 Å, no apparent charge density change has been observed.

With 1 ML Mg residing at the GB, one can find a charge density depletion between atoms Al(2) and Al(-2) in Fig. 10, which indicates a weakening of the primary bond Al(2)-Al(-2), in comparison to the pristine Σ5 (210) STGB. Such a weakening can also be seen for the bonds of Mg-Al(2) and Mg-Al(4). Charge density depletion induced by Mg segregation across the Al GB has also been reported by Zhang et al. [49] and Liu et al. [16], suggesting an intrinsic feature of Mg solutes in decreasing the bonding charge density of Al atoms across the GB interface. Given the atomic size of Mg being larger than Al, Mg segregation at site 1 would cause the GB to expand. Therefore, the atomic bonds connecting the micro grains across the GB would be elongated. Calculations reveal that 1 ML Mg segregation would produce an expansion of the GB by 0.23 Å and stretch the primary Al(2)-Al(-2) bond length by 3.6%, Mg-Al(2) and Mg-Al(4) bonds by 16%, relative to pristine Σ5 (210) STGB. As a consequence of this expansion, the strength of atomic bonds connecting the two micro grains in the vicinity of GB would be weakened, resulting in a decreased overall strength of the GB.

Apart from the atomic size effect, Mg possessing smaller number of valence electrons could be another cause for the considerably decreased charge density around Mg atom (cf. Fig. 10) at the GB. As displayed in Fig. 10, the critical elongation prior fracture of GB/1ML-Mg during uniaxial tensile test is 2.1 Å, a little larger than that of pristine Σ5 (210) STGB (2 Å). This is an indication of the less rigid and stiff interatomic bonds across the Mg segregated GB, as evidenced in Section D.

On the contrary, the segregation of interstitial Cu would enormously increase the charge density across the GB and three new atomic bonds connecting Cu-Al(1), Cu-Al(3), Cu-Al(-3) are formed (cf. Fig. 11). Cu segregation would also result in the expansion of Σ5 (210) STGB since there is no sufficient space at the hollow site to accommodate Cu solute atoms. The calculations reveal that 1ML Cu coverage would cause the GB to expand by 0.89 Å. As expected, this GB expansion significantly elongates the bonds connecting the micro grains, i.e. Al(2)-Al(-2) from 2.58 to 2.83 Å, Al(1)-Al(2) from 2.94 to 2.98 Å, Al(1)-Al(4) from 3.13 to 3.35 Å. An increased length would represent weakening of these interatomic bonds, which is validated by the depletion of charge density for these bonds in the charge plot of 0.0 Å in Fig. 11. In addition, the present calculations show that the newly formed Cu-Al(3) bond exhibits a maximum binding charge of 0.042 $e/bohr^3$, which is nearly as high as that of the primary Al(2)-Al(-2) bond prior bond elongation. However, as a result of GB expansion, the maximum charge density of the primary Al(2)-Al(-2) bond only decreases by 0.12 $e/bohr^3$, much smaller than the bonding charge of Cu-Al(3). Although a slight weakening of original bonds like Al(2)-Al(-2), etc., occurs at the GB, the overall strength of GB/1ML-Cu can be improved by the newly formed Cu-Al bonds. It is thus clarified that the strengthening effect of Cu upon Σ5 (210) STGB lies in creating new atomic bonding across the GB, which is as strong as the primary Al(2)-Al(-2) bond prior elongation and hence increases GB cohesion and its resistance against intergranular fracture.

One can find in Fig. 11 that the fracture process of GB/1ML-Cu is distinct and more complex relative to the pristine Σ5 (210) STGB and GB/1ML-Mg. As shown in Fig. 11, the system is elastically elongated at the beginning, and the charge density of the bonds connecting the micro grains decreases with the increase of displacement, indicating a stretch-induced weakening. All the atomic

bonds remains connected till a displacement of 2.2 Å. The first fracture occurs for bonds of Cu-Al(3), Al(2)-Al(-2) between displacement 2.2 and 2.3 Å. These two bonds are considered to have a large contribution to the bonding strength of GB/1ML-Cu. This is consistent with the prediction that the σ_{max} of GB/1ML-Cu is at the displacement of 2.2 Å (cf. Fig. 8), which is exactly prior to the fracture of Cu-Al(3), Al(2)-Al(-2) bonds. After the breaking of Cu-Al(3), Al(2)-Al(-2) bonds, the GB is not completely split up, but still stays connected via the Al(1)-Al(2) bond until a further displacement of 2.6 and 2.7 Å. Apparently, the newly formed Cu-Al bonds allow GB/1ML-Cu to bear a larger stretch since the complete fracture needs additional steps and elongation. It is now clear that the complex process for complete cleavage of GB/1ML-Cu involves a two-step fracture of the atomic bonds holding the GB. Through creating additional Cu-Al bonds across the GB, interstitial Cu not only increases the theoretical strength of Σ5 (210) STGB, but also enables it to sustain larger elongation.

4. Discussion

Given the fact that Mg solubility in Al is large (18.6 at.% Mg at 723 K), the segregation tendency of Mg solutes towards Al GB is still tremendous. As demonstrated, our calculations are in agreement with the results which have been well established both experimentally [5-10] and theoretically [14-18] that Mg is prone to segregate to Al GBs. Using Atom Probe Tomography (APT), Sauvage et al. [59] confirmed a nearly 20 at.% local enrichment of Mg along the GBs in Al-Mg alloys processed by severe plastic deformations. However, evident controversies persist upon the effect of Mg towards the cohesion strength of Al GBs [13-18]. These controversial results can be attributed to the different fracture models (Griffith, Rice-Wang, etc.) utilized for the description of GB cohesion strength, as well as the distinct GB structures investigated in these works. As postulated by Bauer et al. [31], Seah [60], Hirth and Rice [61], Lozovoi et al. [62], to depict the GB decohesion process, there are two theoretical models, i.e. canonical (Griffith) and grand-canonical (Rice-Wang) formulations. The Griffith model is applicable when the crack growth of the GB is so fast compared with the diffusion rate of impurities, so that the system is not able to equilibrate instantly. Thereby, the impurity atoms residing at the fractured surfaces shall come exclusively from the GB interface. On the contrary, mobile solutes with a high diffusivity enable the system to reach a local equilibrium rapidly

to maintain constant chemical potential of the solutes during the crack growth, for instance, the hydrogen embrittlement [63]. In this situation, the fracture behavior of GB can be well depicted within Rice-Wang formulation. It is demonstrated by Bauer et al. [31] that the sensitivity of GB towards embrittlement has a strong dependency upon the selection of theoretical models of decohesion. Nevertheless, with a much lower diffusivity than H [64, 65], Mg is not deemed as a mobile segregation candidate in Al matrix, and thereby the fracture behavior of GBs segregated with Mg solutes would very much favor a canonical Griffith interpretation of the thermodynamic formulation for interfacial decohesion. This is also the reason why a comprehensive Griffith fracture analysis has been implemented upon Al Σ5 (210) STGB with Mg segregation in the present work. With a combined methodology of Griffith model and *ab-initio* tensile test, we have clarified the Mg embrittling effect upon Al Σ5 (210) STGB as being a combined result of "structural effect" – GB expansion ascribed to the larger atomic size of Mg and "chemical effect" – charge density depletion. Indeed, this embrittling effect of Mg solutes has been experimentally observed in hot working or cyclic creep of Al–Mg alloys [66, 67], in which segregated Mg solutes seem to cause GB cracking and have the effect of decreasing the cohesive strength of Al GBs.

The remarkable segregation of Cu solutes towards Al GBs has been recognized in a variety of experiments. A three-dimensional atom probe investigation, as done by Sha et al. [12], of an UFG Al–Zn–Mg–Cu alloy subjected to equal-channel angular pressing (ECAP) shows the strong segregation of Cu solutes towards Al GBs, being consistent with our present findings. In addition, the strong interstitial-site segregation behavior of Cu solutes towards Al Σ5 (310)/[001] GBs has been revealed by Campbell et al. [68] and Liu et al. [69], which is similar to the preferential interstitial segregation of Cu towards Al Σ5 (210) STGB as determined in this work. Cu solutes are demonstrated to be a cohesion enhancer for Al GBs in the present work. Actually, the adhesion-enhancing mechanism of Cu is analogous to the strengthening effect of B towards Al Σ5 (210) STGB [17], both of which create additional new atomic bonds across the GB, resulting in an enhanced boundary strength. However, a notable difference would exist in the nature of the newly-formed atomic bonds. Apparently, Cu would favor a metallic bonding character with surrounding Al atoms at the GB, while B exhibits a mixed

bonding nature [17] – metallic interplayed with covalent. Apart from this, the structural effect of Cu solutes upon Al Σ5 (210) STGB is more significant than B. As a small atom, the interstitial segregation of B at hollow site does not cause structural expansion of the GB, as indicated by Zhang at al. [17]. However, the GB hollow site cannot hold a larger Cu atom and thereby has to expand to accommodate its segregation, resulting in a negative structural contribution to the GB strength. Still, the segregation of Cu solutes may also affect other GB properties, e.g. diffusion, electromigration, etc. [68], which are complex issues and will be addressed in our future work.

5. Conclusions

A comprehensive and systematic first-principles study was conducted to investigate the Mg, Cu segregation and their effects upon Σ5 (210)[001] STGB in Al. Both Mg and Cu solutes were found to have a large driving force to segregate to Al GBs. It is shown that Mg solutes prefer to segregate at symmetric substitutional core segregation sites, while Cu prefers segregation at interstitial hollow sites at the GB. A more negative segregation energy of Cu than Mg impurities suggests that Al Σ5 (210)[001] STGB is more attractive for the segregation of Cu impurities. The segregation of Mg and Cu impurities can both result in a GB expansion and a significant decrease in the GB energy of Al Σ5 (210)[001] STGB. Based on the canonical Griffith fracture model aided with ab-initio tensile test calculations, we confirm that Mg solutes have an embrittling effect on Al Σ5 (210)[001] STGB. A detailed analysis of the GB structures, theoretical strength-displacement curves, and charge density evolution during uniaxial tensile test reveals that the Mg decohesion effect upon Al Σ5 (210) STGB is a combined result of "structural effect"- GB expansion and "chemical effect"-charge density depletion. On the contrary, Cu solutes were shown to be a cohesion enhancer for Al GBs. Calculations uncover that this strengthening effect of Cu solutes results from the creation of new Cu-Al bonds across the GB. In spite of the negative structural contribution of Cu impurities, the newly formed Cu-Al bonds are considered to have a strong strength contribution to the Al GB and thus increase its resistance against intergranular fracture.

Acknowledgements

References

[1] P.V. Liddicoat, X.-Z. Liao, Y.H. Zhao, Y.T. Zhu, M.Y. Murashkin, E.J. Lavernia, R.Z. Valiev, S.P. Ringer, Nanostructural hierarchy increases the strength of aluminium alloys, Nat. Commun., 1 (2010) 63.

[2] A. Khalajhedayati, Z.L. Pan, T.J. Rupert, Manipulating the interfacial structure of nanomaterials to achieve a unique combination of strength and ductility, Nat. Commun., 7 (2016) 10802.

[3] D. Raabe, M. Herbig, S. Sandlöbes, Y. Li, D. Tytko, M. Kuzmina, D. Ponge, P.-P. Choi, Grain boundary segregation engineering in metallic alloys: A pathway to the design of interfaces, Curr. Opin. Solid. State. Mater Sci., 18 (2014) 253–261.

[4] Y. Li, D. Raabe, M. Herbig, P. Choi, S. Goto, A. Kostka, H. Yarita, C. Borchers, R. Kirchheim, Segregation Stabilizes Nanocrystalline Bulk Steel with Near Theoretical Strength, Phys. Rev. Lett., 113 (2014) 106104.

[5] D.R. Baer, C.F. Windisch, M.H.E. Jr., M.J. Danielson, R.H. Jones, J.S. Vetrano, Influence of Mg on the corrosion of Al, J. Vac. Sci. Technol. A, 18 (1999) 131-136.

[6] J.M. Chen, T.S. Sun, R.K. Viswanadham, J.A.S. Green, Grain Boundary Segregation of an Al-Zn-Mg Ternary Alloy, Metall. Trans. A, 8A (1977) 1935-1940.

[7] J.R. Pickens, T.J. Langan, The Effect of Solution Heat-Treatment on Grain Boundary Segregation and Stress-Corrosion Cracking of Al-Zn-Mg Alloys, Metall. Trans. A, 18A (1985) 1735-1744.

[8] P. Doig, J.W. Edington, The Influence of Quenching on the Segregation of Magnesium to the Grain Boundaries in an Al-5.9 Wt Pct Zn-3.2 Wt Pct Mg Alloy, Metall. Trans. A, 6A (1974) 943-945.

[9] R.H. Jones, D.R. Baer, M.J. Danielson, J.S. Vetrano, Role of Mg in the Stress Corrosion Cracking of an Al-Mg Alloy, Metall. Mater. Trans. A, 32A (1999) 1699-1711.

[10] T. Malis, M.C. Chaturvedi, Grain-boundary segregation in an Al-8 wt % Mg alloy, J. Mater. Sci., 17 (1982) 1479-1486.

[11] G. Sha, R.K.W. Marceau, X. Gao, B.C. Muddle, S.P. Ringer, Nanostructure of aluminium alloy 2024: Segregation, clustering and precipitation processes, Acta. Mater., 59 (2011) 1659–1670.

[12] G. Sha, L. Yao, X. Liao, S.P. Ringer, Z.C. Duan, T.G. Langdon, Segregation of solute elements at grain boundaries in an ultrafine grained Al–Zn–Mg–Cu alloy, Ultramicroscopy, 111 (2011) 500-505.

[13] R.G. Song, M.K. Tseng, B.J. Zhang, J. Liu, Z.H. Jin, K.S. Shin, Grain boundary segregation and hydrogen-induced fracture in 7050 Aluminium alloy, Acta. Mater., 44 (1996) 3241-3248.

[14] X.-Y. Liu, J.B. Adams, Grain-boundary segregation in Al-10%Mg alloys at hot working temperatures, Acta. Mater., 10 (1998) 3467-3476.

[15] R.G. Song, W. Dietzel, B.J. Zhang, W.J. Liu, M.K. Tseng, A. Atrens, Stress corrosion cracking and hydrogen embrittlement of an Al–Zn–Mg–Cu alloy, Acta. Mater., 52 (2004) 4727–4743.

[16] X.G. Liu, X.W. Wang, J.Y. Wang, H.Y. Zhang, First-principles investigation of Mg segregation at $\Sigma = 11(113)$ grain boundaries in Al, J. Phys.: Condens. Matter, 17 (2005) 4301–4308.

[17] S. Zhang, O.Y. Kontsevoi, A.J. Freeman, G.B. Olson, Cohesion enhancing effect of magnesium in aluminum grain boundary: A first-principles determination, Appl. Phys. Lett., 100 (2012) 231904.

[18] V.I. Razumovskiy, A.V. Ruban, I.M. Razumovskii, A.Y. Lozovoi, V.N. Butrimb, Y.K. Vekilov, The effect of alloying elements on grain boundary and bulk cohesion in aluminum alloys: An ab initio study, Scr. Mater., 65 (2011) 926–929.

[19] M.A. Gibson, C.A. Schuh, Segregation-induced changes in grain boundary cohesion and embrittlement in binary alloys, Acta. Mater., 95 (2015) 145-155.

[20] J.L. Wang, R. Janisch, G.K.H. Madsen, R. Drautz, First-principles study of carbon segregation in bcc iron symmetrical tilt grain boundaries, Acta. Mater., 115 (2016) 259-268.

[21] V.I. Razumovskiy, A.Y. Lozovoic, I.M. Razumovskii, First-principles-aided design of a new Ni-base superalloy: Influence of transition metal alloying elements on grain boundary and bulk cohesion, Acta. Mater., 82 (2015) 369–377.

[22] D. Scheiber, R. Pippanc, P. Puschnig, A. Ruban, L. Romaner, Ab-initio search for cohesion-enhancing solute elements at grain boundaries in molybdenum and tungsten, Int. J. Refract. Met. Hard Mater., 60 (2016) 75-81.

[23] P. Lejček, M. Šob, V. Paidar, Interfacial segregation and grain boundary embrittlement: An overview and critical assessment of experimental data and calculated results, Prog. Mater. Sci., 87 (2017) 83–139.

[24] G. Duscher, M.F. Chisholm, U. Alber, M. Rühle, Bismuth-induced embrittlement of copper grain boundaries, Nature Mater., 3 (2004) 621-626.

[25] R. Schweinfest, A.T. Paxton, M.W. Finnis, Bismuth embrittlement of copper is an atomic size effect, Nature, 432 (2004) 1008-1011.

[26] R.Q. Wu, A.J. Freeman, G.B. Olson, First Principles Determination of the Effects of Phosphorus and Boron on Iron Grain Boundary Cohesion, Science, 265 (1994) 376-380.

[27] W.T. Geng, A.J. Freeman, R. Wu, C.B. Geller, J.E. Raynolds, Embrittling and strengthening effects of hydrogen, boron, and phosphorus on a S5 nickel grain boundary, Phys. Rev. B, 60 (1999) 7149-7155.

[28] S. Zhang, O.Y. Kontsevoi, A.J. Freeman, G.B. Olson, First-principles determination of the effect of boron on aluminum grain boundary cohesion, Phys. Rev. B, 84 (2011) 134104.

[29] A.A. Griffith, The Phenomena of Rupture and Flow in Solids, Philos, Trans. R. Soc. London Ser. A, 221 (1920) 163-179.

[30] J.R. Rice , J.S. Wang, Embrittlement of Interfaces by Solute Segregation, Mater. Sci. Eng. A, 107 (1989) 23-40.

[31] K.-D. Bauer, M. Todorov, K. Hingerla, J. Neugebauer, A first principles investigation of zinc induced embrittlement at grain boundaries in bcc iron, Acta. Mater., 90 (2015) 69–76.

[32] Y. Zhang, G.-H. Lu, S. Deng, T. Wang, H. Xu, M. Kohyama, R. Yamamoto, Weakening of an aluminum grain boundary induced by sulfur segregation: A first-principles computational tensile test, Phys. Rev. B, 75 (2007) 174101.

[33] S. Zhang, O.Y. Kontsevoi, A.J. Freeman, G.B. Olson, First principles investigation of zinc-induced embrittlement in an aluminum grain boundary, Acta. Mater., 59 (2011) 6155–6167.

[34] S. Zhang, O.Y. Kontsevoi, A.J. Freeman, G.B. Olson, Aluminum grain boundary decohesion by dense sodium segregation, Phys. Rev. B, 85 (2012) 214109.

[35] H. Momida, Y. Asari, Y. Nakamura, Y. Tateyama, T. Ohno, Hydrogen-enhanced vacancy embrittlement of grain boundaries in iron, Phys. Rev. B, 88 (2013) 144107.

[36] G. Kresse, J. Furthmüller, Efficiency of ab-initio total energy calculations for metals and semiconductors using a plane-wave basis set, Comp. Mater. Sci., 6 (1996) 15-50.

[37] G. Kresse, J. Furthmüller, Efficient iterative schemes for ab initio total-energy calculations using a plane-wave basis set, Phys. Rev. B, 54 (1996) 11169-11186.

[38] P.E. Blöchl, Projector augmented-wave method, Phys. Rev. B, 50 (1994) 17953-17979.

[39] G. Kresse, D. Joubert, From ultrasoft pseudopotentials to the projector augmented-wave method, Phys. Rev. B, 59 (1999) 1758-1775.

[40] J.P. Perdew, K. Burke, M. Ernzerhof, Generalized Gradient Approximation Made Simple, Phys. Rev. Lett., 77 (1996) 3865.

[41] H.J. Monkhorst, J.D. Pack, Special points for Brillouin-zone integrations, Phys. Rev. B, 13 (1976) 5188-5192.

[42] P.E. Blöchl, O. Jepsen, O.K. Andersen, Improved tetrahedron method for Brillouin-zone integrations, Phys. Rev. B, 49 (1994) 16223-16233

[43] A.M. Tahir, R. Janisch, A. Hartmaier, Ab initio calculation of traction separation laws for a grain boundary in molybdenum with segregated C impurites, Modelling Simul. Mater. Sci. Eng., 21 (2013) 075005.

[44] P. Lazar, R. Podloucky, Cleavage fracture of a crystal: Density functional theory calculations based on a model which includes structural relaxations, Phys. Rev. B, 78 (2008) 104114.

[45] R. Janisch, N. Ahmed, A. Hartmaier, Ab initio tensile tests of Al bulk crystals and grain boundaries: Universality of mechanical behavior, Phys. Rev. B, 81 (2010) 184108.

[46] A.M. Tahir, R. Janisch, A. Hartmaier, Hydrogen embrittlement of a carbon segregated Σ5 310 001 symmetrical tilt grain boundary in α-Fe, Mater. Sci. Eng. A, 612 (2014) 462–467.

[47] G. Lu, N. Kioussis, Interaction of vacancies with a grain boundary in aluminum: A first-principles study, Phys. Rev. B, 64 (2001) 024101.

[48] J.R. Smith, J. Ferrante, Grain-boundary energies in metals from local-electron-density distributions, Phys. Rev. B, 34 (1986) 2238-2245.

[49] S. Zhang, O.Y. Kontsevoi, A.J. Freeman, G.B. Olson, Sodium-induced embrittlement of an aluminum grain boundary, Phys. Rev. B, 82 (2010) 224107.

[50] G.C. Hasson, C. Goux, Interfacial energies of tilt boundaries in aluminium experimental and theoretical determination, Scr. Metall., 5 (1971) 889-894.

[51] L.E. Murr, Twin boundary energetics in pure Aluminium, Acta Metall., 21 (1973) 791-797.

[52] J.H. Rose, J.R. Smith, J. Ferrante, Universal features of bonding in metals, Phys. Rev. B, 28 (1983) 1835-1845.

[53] R. Kirchheim, Reducing grain boundary, dislocation line and vacancy formation energies by solute segregation II. Experimental evidence and consequences, Acta Mater., 55 (2007) 5139–5148.

[54] R. Kirchheim, Reducing grain boundary, dislocation line and vacancy formation energies by solute segregation. I. Theoretical background, Acta Mater., 55 (2007) 5129–5138.

[55] P.C. Millett, R.P. Selvam, A. Saxena, Molecular dynamics simulations of grain size stabilization in nanocrystalline materials by addition of dopants, Acta Mater., 54 (2006) 297–303.

[56] P.C. Millett, R.P. Selvam, S. Bansal, A. Saxena, Atomistic simulation of grain boundary energetics – Effects of dopants, Acta Mater., 53 (2005) 3671–3678.

[57] K. Park, G.H. Paulino, Cohesive Zone Models: A Critical Review of Traction-Separation Relationships Across Fracture Surfaces, Appl. Mech. Rev., 64 (2011) 060802.

[58] M. Černý, P. Šesták, P. Řehák, M.Všianská, M. Šob, Ab initio tensile tests of grain boundaries in the fcc crystals of Ni and Co with segregated sp-impurities, Mater. Sci. Eng. A, 669 (2016) 218–225.

[59] X. Sauvage, N. Enikeev, R. Valiev, Y. Nasedkina, M. Murashkin, Atomic-scale analysis of the segregation and precipitation mechanisms in a severely deformed Al–Mg alloy, Acta Mater, 72 (2014) 125–136.

[60] M.P. Seah, Segregation and the Strength of Grain Boundaries., Proc. R. Soc. Lond. A, 349 (1976) 535-554.

[61] J.P. Hirth, J.R. Rice, On the thermodynamics of adsorption at interfaces as it influences decohesion, Metall. Trans. A, 11 (1980) 1501-1511.

[62] A.Y. Lozovoi, A.T. Paxton, M.W. Finnis, Structural and chemical embrittlement of grain boundaries by impurities: A general theory and first-principles calculations for copper, Phys. Rev. B, 74 (2006) 155416.

[63] M. Yamaguchi, K.-I. Ebihara, M. Itakura, T. Kadoyoshi, T. Suzudo, H. Kaburaki, First-Principles Study on the Grain Boundary Embrittlement of Metals by Solute Segregation: Part II. Metal (Fe, Al, Cu)-Hydrogen (H) Systems, Metall. Mater. Trans. A, 42A (2011) 330-339.

[64] G.A. Young JR, J.R. Scully, The diffusion and trapping of hydrogen in high purity Aluminium, Acta. Mater., 46 (1998) 6337-6349.

[65] Y. Du, Y.A. Chang, B. Huang, W.P. Gong, Z.P. Jin, H.H. Xu, Z.H. Yuan, Y. Liu, Y.H. He, F.-Y. Xie, Diffusion coefficients of some solutes in fcc and liquid Al: critical evaluation and correlation, Mater. Sci. Eng. A, 363 (2003) 140-151.

[66] H. Wang, M. Kohyama, S. Tanaka, Y. Shiihara, First-principles study of Si and Mg segregation in grain boundaries in Al and Cu: application of local-energy decomposition, J. Mater. Sci., 50 (2015) 6864-6881.

[67] S.H. Na, M.S. Yang, S.W. Nam, Effects of stress amplitude and internal stress on the grain boundary deformation behavior under high temperature creep in an Al-2.9%Mg alloy, Scr. Mater., 32 (1995) 627–632.

[68] G.H. Campbell, J.M. Plitzko, W.E. King, Copper Segregation to the Σ5 (310)/[001] Symmetric Tilt Grain Boundary in Aluminum, Interf. Sci., 12 (2004) 165–174.

[69] X.-Y. Liu, C.-L. Liu, L.J. Borucki, A new investigation of copper's role in enhancing Al–Cu interconnect electromigration resistance from an atomistic view, Acta. Mater., 47 (1999) 3227-3231.

Tables

Table 1. Grain boundary energy γ_{GB} and fracture energy $\Delta\gamma$ of the Σ5 (210)[001] symmetrical tilt grain boundary in Al, and surface energy γ_{surf} of the (210) Al free surface, in comparison with the theoretical and experimental values.

Energy	Value (J/m^2)	Temperature (K)	Method	Reference
γ_{GB}	0.518	0	First-principles	Present Work
	0.501	0	[a]FLAPW	[49]
	0.47	0	First-principles	[18]

	0.502	0	First-principles	[47]
	0.600	0	Variation method	[50]
	0.411	0	[b]LEDD	[48]
	0.324	723	[c]TEM	[51]
	0.380	298	TEM	[51]
γ_{surf}	1.041	0	First-principles	Present Work
	1.016	0	FLAPW	[49]
	0.96	0	First-principles	[18]
	0.980	723	TEM	[51]
	1.150	298	TEM	[51]
[d]$\Delta\gamma$	1.568	0	First-principles	Present Work
	1.531	0	FLAPW	[49]
	1.44	0	First-principles	[18]
	1.92	723	TEM	[51]

[a]Full-potential linearized augmented plane-wave method.

[b]Local-electron-density distributions.

[c]Transmission electron microscopy.

[d]Results predicted from rigid grain shift + subsequent relaxations.

Table 2. Grain boundary energy γ_{GB}, fracture energy $\Delta\gamma$ of the Al Σ5 (210)[001] STGB, as well as STGBs with different coverages (ML) of Mg and Cu. Free surface energy γ_{surf} in of the Al (210) surface with different coverages (ML) of Mg and Cu. The results from rigid grain shift (RGS) and RGS + relaxations approaches are both included.

Boundary	γ_{GB}, J/m^2	γ_{seg}, eV/atom	$\Delta\gamma$, J/m^2		2γ_{surf}, J/m^2	
			RGS	RGS+relaxation	RGS	RGS+relaxation
Al-bulk-(210)-planes	-	-	2.185	2.085	2.167	2.067
Al-Σ5 (210)[001]	0.518	-	1.764	1.568	2.282	2.082
0.25ML-Mg	0.465	-0.255	1.730	1.564	2.195	2.029
0.5ML-Mg	0.406	-0.266	1.710	1.565	2.111	1.972
0.75ML-Mg	0.341	-0.279	1.693	1.575	2.029	1.917
1.0ML-Mg	0.279	-0.284	1.664	1.594	1.937	1.868

0.25ML-Cu	0.375	-0.494	1.852	1.645	2.224	2.015
0.5ML-Cu	0.226	-0.508	1.941	1.724	2.167	1.943
0.75ML-Cu	0.042	-0.561	2.057	1.877	2.100	1.911
1.0ML-Cu	-0.140	-0.587	2.139	2.034	2.000	1.883

Table 3. Fracture strength σ_{th} predicted via rigid grain shift (RGS) and RGS + relaxation methodologies, critical separation, δ_c, final separation, δ_f, of the Al bulk 210 planes, Σ5 (210)[001] STGB, as well as STGBs with different coverages (ML) of Mg and Cu.

Boundary	[a]σ_{th}, GPa	δ_c, (Å)	δ_f, (Å)	[b]σ_{th}, GPa
Al-bulk-(210)-planes	[c]11.96	0.644	3.65	[e]9.39
Al-Σ5 (210)[001]	[d]10.86	0.596	3.25	[f]8.93
0.25ML-Mg	10.33	0.606	3.35	-
0.5ML-Mg	9.78	0.607	3.50	-
0.75ML-Mg	9.33	0.619	3.63	-
1.0ML-Mg	8.88	0.632	3.75	7.79
0.25ML-Cu	11.37	0.614	3.26	-
0.5ML-Cu	11.86	0.622	3.27	-
0.75ML-Cu	12.75	0.607	3.23	-
1.0ML-Cu	13.29	0.623	3.22	10.37

[a]RGS (rigid grain shift).

[b]RGS (rigid grain shift) + relaxation.

[c]The theoretical strength of Al-bulk-(210)-planes from Zhang et al. [49] is 11.6 GPa.

[d]The theoretical strength of pristine Σ5 (210) STGB from Zhang et al. [49] is 10.6 GPa.

[e]The theoretical strength of Al-bulk-(210)-planes from Zhang et al. [49] is 8.4 GPa.

[f]The theoretical strength of pristine Σ5 (210) STGB from Zhang et al. [49] is 7.9 GPa.

Figures
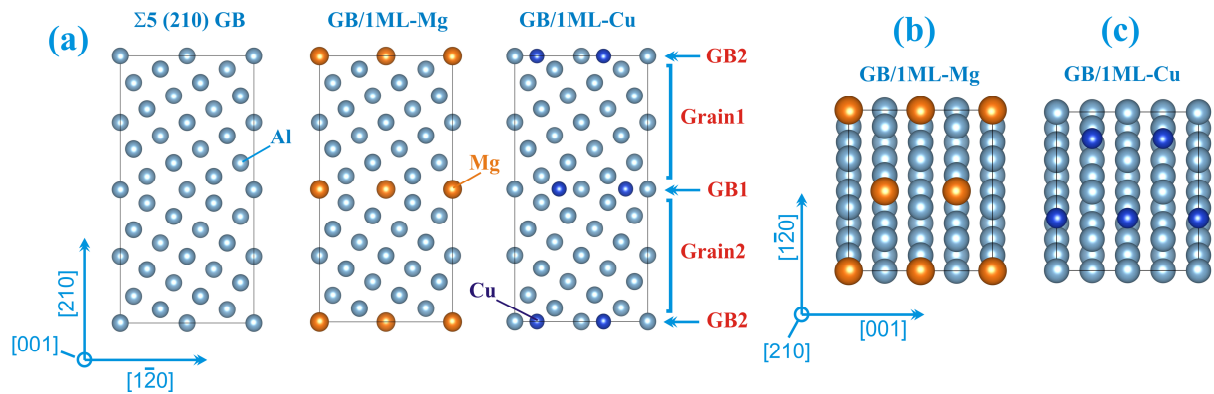
Fig. 1. (a) Crystal structures of the Al Σ5 (210)[001] pristine STGB, and GBs with 1 monolayer (ML) Mg (GB/1ML-Mg) and Cu (GB/1ML-Cu) coverage. The Al, Mg and Cu atoms are as indicated. The two GBs (GB1, GB2) and micro grains (Grain1, Grain2) are also depicted. (b) Al Σ5 (210)[001] STGB plane having one monolayer (1ML) Mg segregation. (c) Al Σ5 (210)[001] STGB plane having one monolayer (1ML) Cu segregation.
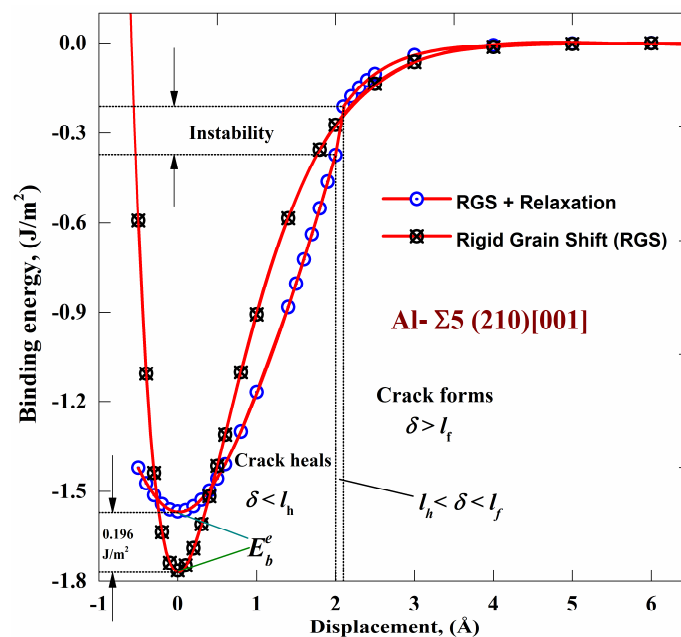

Fig. 2. Binding energy versus displacement curves of pristine Al Σ5 (210)[001] STGB, evaluated in the rigid grain shift (RGS) and RGS + relaxation methodology. The vertical dot line l_h represents the critical displacement, below which the crack can be healed via elastic relaxations. The vertical dot line

l_f represents the crack formation displacement. The instability region of interval crack openings between l_h and l_f is also sketched.
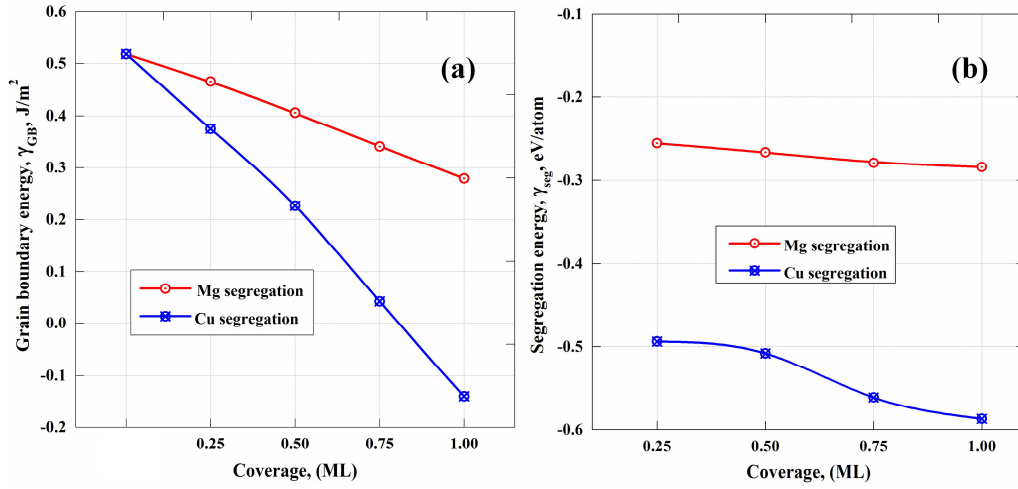
Fig. 3. (a) Grain boundary energy, γ_{GB} of Al $\Sigma5$ (210)[001] STGBs and (b) segregation energy, γ_{seg} as a function of Mg and Cu coverage, respectively.
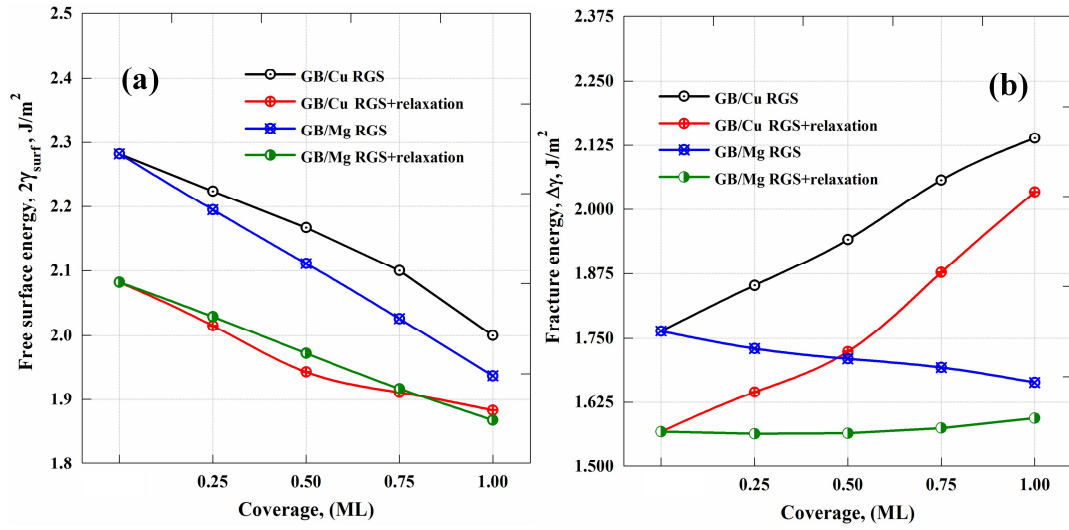
Fig 4. (a) Free surface energy, $2\gamma_{surf}$, of Al (210) surface and (b) fracture energy, $\Delta\gamma$, of Al $\Sigma5$ (210)[001] STGBs as a function of Mg and Cu coverage, respectively.
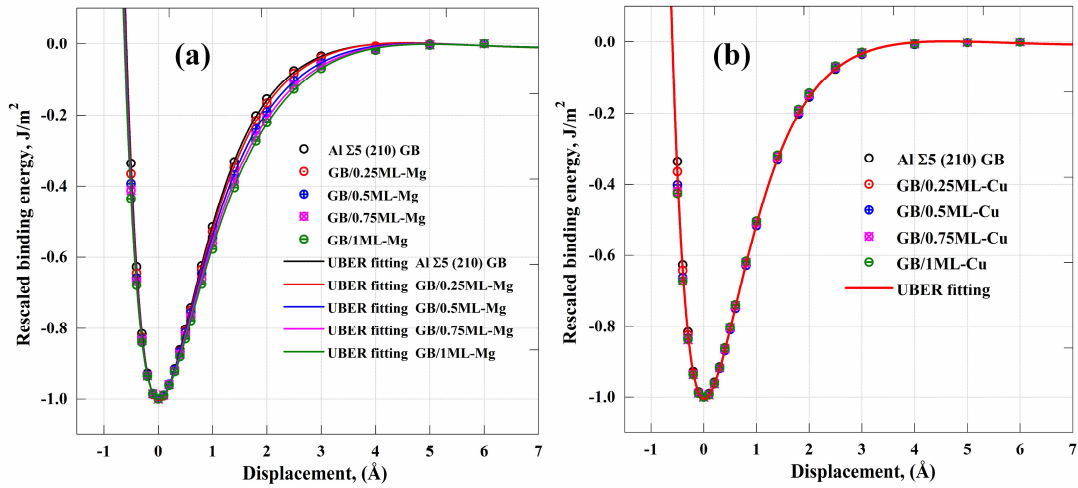
Fig. 5. The rescaled binding energy displacement curves of Mg (a) and Cu (b) segregated Al Σ5 (210)[001] STGBs, which is evaluated via rigid grain shift (RGS) methodology. The UBER fittings are also included.
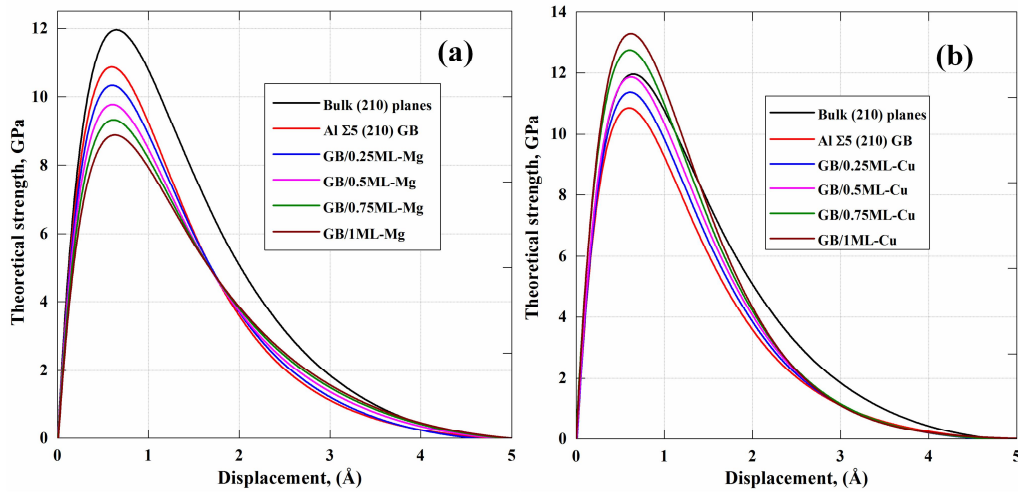
Fig. 6. Theoretical strength of Mg (a) and Cu (b) segregated Al Σ5 (210)[001] STGBs, as well as Al bulk (210) planes as a function of displacement, obtained in the rigid grain shift (RGS) methodology.
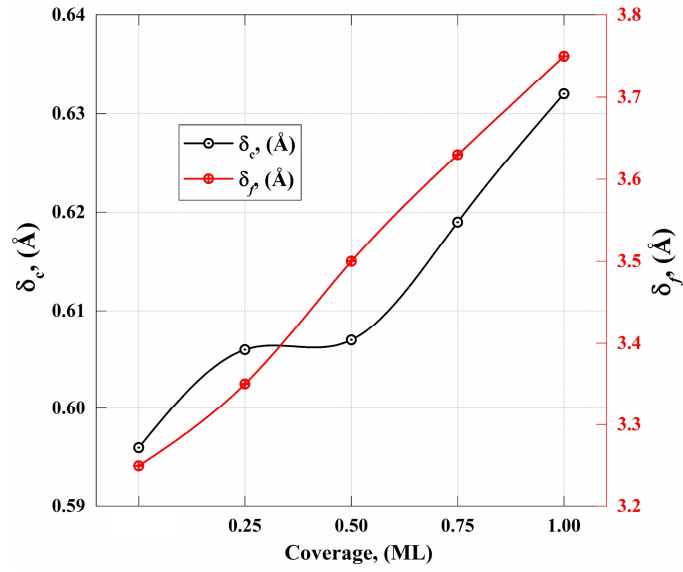
Fig. 7. Critical separation δ_c and final separation δ_f for Al Σ5 (210)[001] STGBs as a function of Mg coverage.
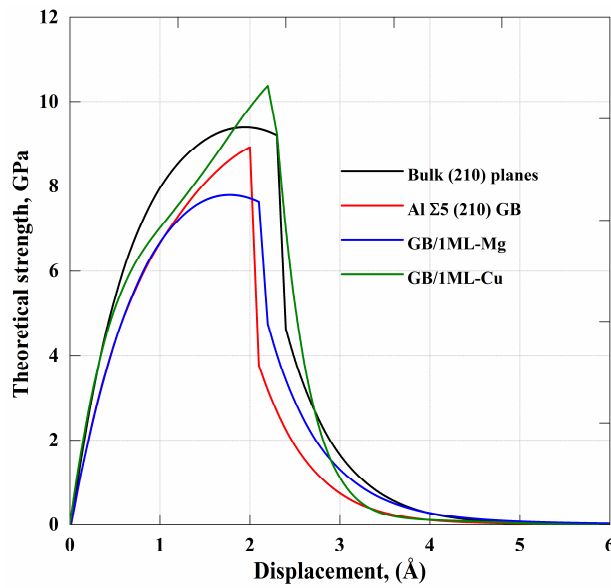
Fig. 8. Theoretical strength of Al bulk (210) planes, Al Σ5 (210)[001] STGB, GB/1ML-Mg and GB/1ML-Cu, predicted within the rigid grain shift (RGS) + relaxation methodology.
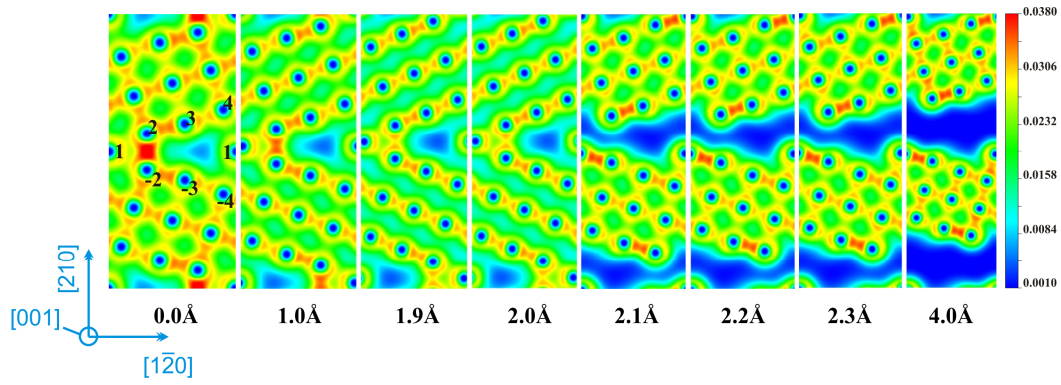
Fig. 9. Calculated charge density distributions of pristine Al Σ5 (210)[001] STGB in the [001] plane, along with the increased displacement distance, evaluated in the rigid grain shift (RGS) + relaxation methodology. The unit is in *e/bohr³*.
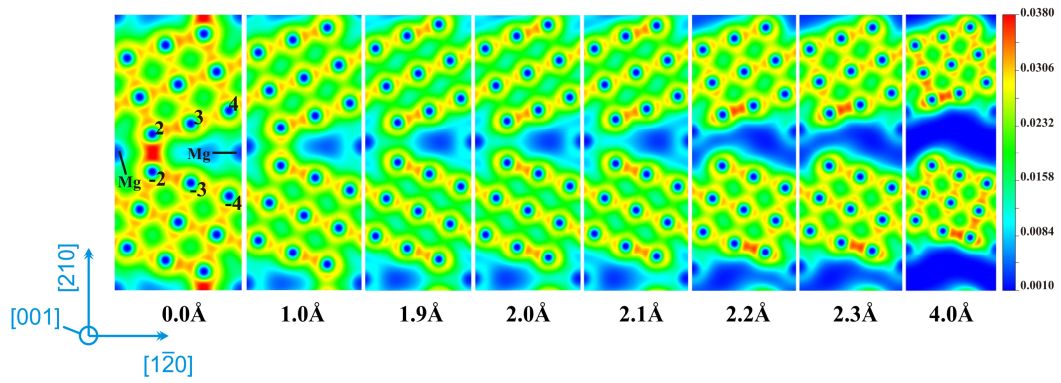

Fig. 10. Calculated charge density distributions of GB/1ML-Mg in the [001] plane, along with the increased displacement distance, evaluated in the rigid grain shift (RGS) + relaxation methodology. The unit is in *e/bohr³*.
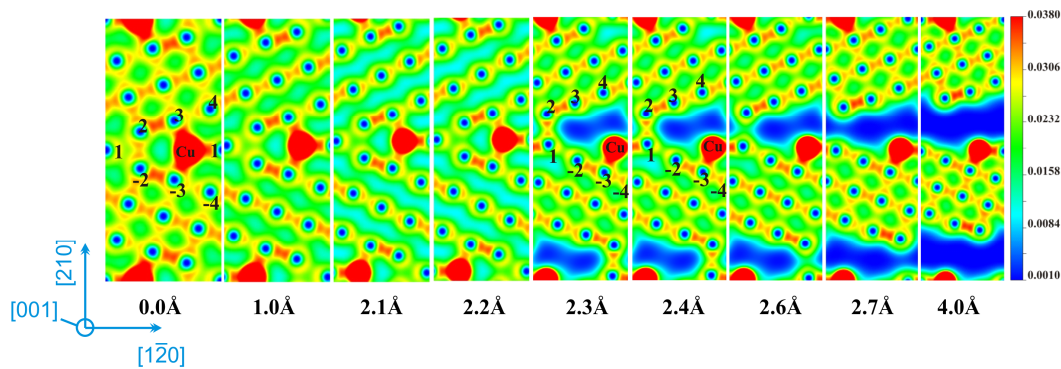
Fig. 11. Calculated charge density distributions of GB/1ML-Cu in the [001] plane, along with the increased displacement distance, evaluated in the rigid grain shift (RGS) + relaxation methodology. The unit is in *e/bohr³*.